Stellar reaction rate for ^{22}Mg + $p \rightarrow$ ^{23}Al from the asymptotic normalization coefficient in the mirror nuclear system ^{22}Ne + $n \rightarrow$ ^{23}Ne

T. Al-Abdullah,[1,2,*] F. Carstoiu,[3] X. Chen,[1,†] H. L. Clark,[1] C. Fu,[1,‡] C. A. Gagliardi,[1] Y.-W. Lui,[1] A. Mukhamedzhanov,[1] G. Tabacaru,[1] Y. Tokimoto,[1] L. Trache,[1] and R. E. Tribble[1]

[1]*Cyclotron Institute, Texas A&M University, College Station, Texas 77843, USA*

[2]*Physics Department, The Hashemite University, Zarqa 13115, Jordan*

[3]*National Institute for Physics and Nuclear Engineering "Horia Hulubei," R-76900 Bucharest-Magurele, Romania*

(Received 25 August 2009; revised manuscript received 7 November 2009; published 19 March 2010)

The production of ^{22}Na in ONe novae can be influenced by the ^{22}Mg$(p,\gamma)^{23}$Al reaction. To investigate this reaction rate at stellar energies, we have determined the asymptotic normalization coefficient (ANC) for ^{22}Mg + $p \rightarrow$ ^{23}Al through measurements of the ANCs in the mirror nuclear system ^{22}Ne + $n \rightarrow$ ^{23}Ne. The peripheral neutron-transfer reactions ^{13}C(^{12}C,^{13}C)^{12}C and ^{13}C(^{22}Ne,^{23}Ne)^{12}C were studied. The identical entrance and exit channels of the first reaction make it possible to extract independently the ground-state ANC in ^{13}C. Our experiment gives $C^2_{p_{1/2}}(^{13}\mathrm{C}) = 2.24 \pm 0.11$ fm^{-1}, which agrees with the value obtained from several previous measurements. The weighted average for all the obtained $C^2_{p_{1/2}}$ is 2.31 ± 0.08 fm^{-1}. This value is adopted to be used in obtaining the ANCs in ^{23}Ne. The differential cross sections for the reaction ^{13}C(^{22}Ne,^{23}Ne)^{12}C leading to the $J^\pi = 5/2^+$ and $1/2^+$ states in ^{23}Ne have been measured at 12 MeV/u. Optical model parameters for use in the DWBA calculations were obtained from measurements of the elastic scatterings ^{22}Ne + ^{13}C and ^{22}Ne + ^{12}C. The extracted ANC for the ground state in ^{23}Ne, $C^2_{d_{5/2}} = 0.86 \pm 0.08 \pm 0.12$ fm^{-1}, is converted to its corresponding value in ^{23}Al using mirror symmetry to give $C^2_{d_{5/2}}(^{23}\mathrm{Al}) = (4.63 \pm 0.77) \times 10^3$ fm^{-1}. The astrophysical S factor $S(0)$ for the ^{22}Mg(p,γ) reaction was determined to be 0.96 ± 0.11 keV b. The consequences for nuclear astrophysics are discussed.

DOI: 10.1103/PhysRevC.81.035802 PACS number(s): 26.30.−k, 21.10.Jx, 25.70.Hi, 27.30.+t

I. INTRODUCTION

Classical novae are relatively common events in our galaxy, with models predicting about 30 yr^{-1}, and with a few per year actually being detected. This large frequency of appearance increases the possibility of studying them by observations in various parts of the electromagnetic spectrum. They are targets of many theoretical models. The current understanding is that they occur in interacting binary systems where H-rich material accretes on a white dwarf from its low-mass main sequence companion. At some point in the accretion the H-rich matter compresses and leads to a thermonuclear runaway during which nucleosynthesis occurs [1]. Once the dynamics of nova outbursts and the nucleosynthesis fueling it are understood, their contribution to the chemical evolution of the galaxy can be better assessed through the comparison of predictions with observations. Novae are believed to become the first type of explosive phenomena where all nuclear data for nucleosynthesis will be based on experimental data [2].

The theoretical and astrophysical analysis of the spectroscopic lines reveals that novae can occur in two types of white dwarfs, carbon-oxygen (CO) and oxygen-neon (ONe). Approximately one-third of all the recently detected novae are ONe novae [3]. The neon concentration of these events in comparison with the solar system abundance is larger by a factor of ∼300 [4]. Moreover, the enrichment of ^{22}Ne in the so-called "Ne-E meteorites," which contain grains that might be partially condensed in nova outbursts, provides evidence of the pre-existence of sodium isotopes, namely ^{22}Na [5,6]. Taken all together, the above observations support the theory that the H-burning sequence of reactions can yield substantial concentrations of ^{22}Na in ONe novae, which is produced in the thermonuclear runaway during the high-temperature stage of the burning region mainly through the reaction chain ^{20}Ne$(p,\gamma)^{21}$Na$(p,\gamma)^{22}$Mg$(\beta^+\nu)^{22}$Na. Then the radioactive ^{22}Na becomes a stalling point because of its slow decay rate to ^{22}Ne via the reaction $^{22}\mathrm{Na} \rightarrow {}^{22}\mathrm{Ne} + \beta^+ + \nu$. The half-life of ^{22}Na is $t_{1/2} = 2.603$ yr. Its β^+ decay populates the short-lived first excited state in ^{22}Ne and leads to the emission of an identifying 1.275-MeV γ ray. If the material is ejected before competing reactions deplete ^{22}Na, then it can be recognized by γ-ray telescopes. Moreover, because of its relatively short lifetime, ^{22}Na can give information about the distribution of matter produced in novae shortly after the outburst, complementary to that given by longer-lived isotopes like ^{26}Al.

It is estimated that for a typical ONe nova the ejected ^{22}Na mass is likely to be on order of $10^{-8} M_\odot$ [7]. For novae in our galactic vicinity, this predicted amount is within the sensitivity limit of the space-based γ-ray telescopes, such as the Compton Gamma Ray Observatory (CGRO) [8] and INTEGRAL [9]. However, observations of five ONe novae using CGRO have not found the signature of these γ rays and have only been able

*abdullatq@comp.tamu.edu

†Present address: Department of Chemistry, Washington University at St. Louis, MO, USA.

‡Present address: National Institute of Standards and Technology (NIST), Gaithersburg, MD, USA.

to set an upper limit for its ejecta, which is below the theoretical estimations [7]. The nuclear data for nucleosynthesis in novae have come under scrutiny as one possible explanation for the missing flux of ^{22}Na γ rays. Studies of the reaction rate for ^{21}Na$(p,\gamma)^{22}$Mg with the DRAGON recoil separator at TRIUMF [10,11] show that the production of ^{22}Na is favored at the early stages in the outburst of ONe white dwarfs, when the temperature and density in the expanding envelope are still high enough to enhance further proton captures on ^{22}Na. As a result, this reduces its final content in the ejecta. Once ^{22}Mg is produced, two reaction paths are accessible. Either it β^+ decays to produce ^{22}Na, which may further capture a proton via the reaction ^{22}Na$(p,\gamma)^{23}$Mg—this reaction is considered as the main depletion candidate [12]—or ^{22}Mg itself is depleted through proton capture ^{22}Mg$(p,\gamma)^{23}$Al. The contribution of this reaction is not clear now. We study this reaction in this article. The low proton-binding energy, which makes photodisintegration of ^{23}Al easily equilibrate p capture, suggests a small contribution, but in nonequilibrium explosive conditions, enough ^{23}Al could be made to allow for a further proton capture into ^{24}Si, and the reaction may contribute this way to ^{22}Na depletion [2,13].

Direct measurements of the ^{22}Mg$(p,\gamma)^{23}$Al reaction at stellar energies have not been possible because of several difficulties. It is impossible to make a ^{22}Mg ($t_{1/2} = 3.86$ s) target and is yet difficult to obtain an intense ^{22}Mg beam for direct measurements in inverse kinematics. However, radiative proton-capture reactions are naturally peripheral at energies of astrophysical interest, so the reaction cross section can be reliably determined from information about the bound wave function of the captured proton at large distances from the core. Hence, we use here an alternative method to determine the rate of the ^{22}Mg$(p,\gamma)^{23}$Al reaction by applying the ANC method [14]. Frequently, this method uses peripheral one-proton transfer reactions to extract the ANC. For our case of ^{23}Al that would require a (^{22}Mg,^{23}Al) reaction, involving again the difficult-to-make ^{22}Mg beam. We overcome this problem by studying instead the mirror neutron-transfer reaction (^{22}Ne,^{23}Ne) and using charge symmetry. The method was first used for the ^{8}B-^{8}Li mirror pair in Ref. [15] and later extended in Ref. [16].

^{23}Al is a weakly bound proton-rich nucleus close to the drip line. An experimental study of the β decay of a pure sample of ^{23}Al has determined the absolute branching ratios and ft values for transitions to states in ^{23}Mg and has confirmed unambiguously that the ground state in ^{23}Al has $J^\pi = 5/2^+$ [17]. Hence, its first excited state must be $1/2^+$, the same as those of corresponding states in the mirror nucleus ^{23}Ne. Moreover, charge symmetry of the nuclear forces implies that the spectroscopic factors of mirror states are the same, and correspondingly the ratio between their ANCs is independent of the nucleon-nucleon force. The difference in the value of the ANCs is attributable to the presence or absence of the Coulomb potential in the outer part of the radial wave functions. Hence, the proton-capture reaction $^{22}\mathrm{Mg} + p \rightarrow {}^{23}$Al can be studied with its mirror neutron-transfer reaction $^{22}\mathrm{Ne} + n \rightarrow {}^{23}$Ne using a stable beam and target. This allows us to populate the $5/2^+$ and $1/2^+$ states in ^{23}Ne and measure their angular distributions with sufficient resolution. The ANCs of these states are extracted and the one for the ground state is converted to its corresponding state of ^{23}Al. The nucleus ^{23}Ne is located in a mass region near the beginning of the *sd* shell that has received significant attention for obtaining a good microscopic description of its nuclear structure. Several studies were dedicated to determining the spectroscopic factors for the states in ^{23}Ne, mainly bound d-wave and s-wave states. Both pickup and stripping reactions have been performed in the form of (p,d) and (d,p) reactions, respectively [18,19]. However, the ANCs for the same states in ^{23}Ne have not been extracted experimentally prior to this work. We present determinations of the ANCs for the ground state and first excited state in ^{23}Ne using the neutron-transfer reaction ^{13}C(^{22}Ne,^{23}Ne)^{12}C. To interpret the results, the ANC for the other vertex $^{13}\mathrm{C} \rightarrow {}^{12}\mathrm{C} + n$ is needed. The ANC for the ground state of ^{13}C has been obtained in several previous works using exchange, (d,p), and (d,t) reactions in direct and inverse kinematics (see Refs. [20,21]). We have performed a complementary study of the neutron-exchange reaction ^{13}C(^{12}C,^{13}C)^{12}C, also reported in this article. The experimental results are interpreted using distorted-wave Born-approximation (DWBA) calculations, for which we need reliable optical model potentials (OMPs). Therefore, we have also measured elastic scattering in an extended angular range and give considerable attention to obtaining OMPs through a phenomenological analysis and using a semimicroscopic double-folding procedure.

We present the details of the two experiments in Sec. II. That is followed in Sec. III by the analysis of elastic-scattering data to obtain the optical model parameters that are used in the DWBA calculations. In Sec. IV the results of the transfer reactions are used to extract the ANCs. These are finally inserted in model calculations to evaluate the radiative capture reaction in Sec. V. The conclusions are summarized in Sec. VI.

II. THE EXPERIMENT

Two experiments were carried out at the Texas A&M University K500 superconducting cyclotron to measure the reactions ^{13}C(^{12}C,^{13}C)^{12}C and ^{13}C(^{22}Ne,^{23}Ne)^{12}C. The energy of the beam was 12 MeV/A for ^{22}Ne and 10.6 MeV/A for ^{12}C, energies for which the reaction mechanism is mostly peripheral. After accelerating the ionized beam in the cyclotron, it was transported through the beam analysis system [22] to control its energy and angular resolution and suppress slit-scattered particles. The angular spread of the beam on the target was less than $\Delta\theta = 0.1^\circ$. The multipole-dipole-multipole (MDM) spectrometer [23] was used to separate the reaction products. We measured the neutron pickup from the loosely bound nucleus ^{13}C and the elastic-scattering cross sections for each reaction. The experimental setup was identical to the one described in Ref. [24]. For this work, the spectrometer's entrance aperture was set at $\Delta\theta = 4^\circ$ (horizontal) and $\Delta\varphi = 1^\circ$ (vertical). The Oxford Detector [25] was used in the focal plane. The entrance and exit windows of the detector were made of Mylar foils, 25 and 50 μm thick, respectively. The windows had large dimensions that allowed for the utilization of the full efficiency of the detector at most of the angles.

Its chamber was filled with pure isobutane gas at a pressure of 30–50 torr. The scattered particles or the reaction products would lose part of their energy in the ionization chamber and then stop completely in a NE102A plastic scintillator, located in air about 42 mm behind the exit window. Four resistive wires are placed in the detector. Their signals were used to determine the position of the particles at different depths. The position resolution was better than 1 mm.

For the ^{22}Ne + C experiments, the elastic-scattering data were measured for the spectrometer angular range $\theta_{\rm lab} = 3^\circ$–$18^\circ$, which is equivalent to the center of mass (c.m.) range $\theta_{\rm c.m.} = 7^\circ$–$49^\circ$, by detecting the ^{22}Ne particles in the focal plane of the spectrometer. Calculations indicate that 96% of the ^{22}Ne were in the +10 charge state at this energy. A correction was applied to account for the remaining 4%. Heavy contaminants in the targets prevented measurements at smaller angles. Two separate runs were performed. The first studied the scattering of ^{22}Ne particles on a nominally 100 μg/cm^2 ^{13}C target; the second studied the scattering of ^{22}Ne particles on a nominally 100 μg/cm^2 ^{12}C target, both self-supporting. Elastic scattering on the first target gives us the OMP needed in the entrance channel of the transfer reaction, while the scattering on the second target allows us to determine the influence of one extra neutron in the target nucleus, because we cannot measure directly the OMP in the exit channel: ^{23}Ne + ^{12}C.

The identification of the particles was achieved by measuring the energy loss in the ionization chamber and the residual energy in the plastic scintillator. Fine-tuned RAYTRACE [26] calculations were used to reconstruct the position of particles in the focal plane and the scattering angle at the target. The target angle reconstruction was checked by measurements with an angle mask consisting of five narrow ($\Delta\theta = 0.1^\circ$) slits in place of the $4^\circ \times 1^\circ$ entrance aperture at several angles of the spectrometer. The overall angular resolution of the experiment was on average $\Delta\theta_{\rm res} = 0.34^\circ$ in the c.m. frame. The spectrometer was moved 2° or 3° at a time to allow for an angle overlap that provided a self-consistency check of the data at all angles. The energy resolution was less than 300 keV. This allowed us to distinguish easily between the position of the 0^+ (ground state), 2^+ (1.275 MeV), and 4^+ (3.358 MeV) states in ^{22}Ne on both ^{13}C and ^{12}C targets, as shown for ^{13}C in Fig. 1. The neutron-transfer reaction ^{13}C(^{22}Ne,^{23}Ne)^{12}C was measured for spectrometer angles 3°, 5°, 7°, and 10° in the laboratory system, which covers the angular range 3°–32° in the c.m. The neutron transfer to the ground and first excited state in ^{23}Ne were detected with a good separation between their positions along the dispersive axis of the MDM focal plane.

Following a similar procedure, the elastic-scattering data for ^{12}C + ^{13}C were measured in the laboratory frame from 3° to 31°, which corresponds to $6^\circ$to 59° in the center-of-mass frame. The inelastic scattering of ^{12}C particles to the first $1/2^+$ excited state in the ^{13}C target was also detected. The ^{13}C(^{12}C,^{13}C)^{12}C exchange reaction measurements were carried out for spectrometer angles 3°–18°, which cover 3°–37° of the angular distribution in the c.m. frame. The transition of a neutron from the ground state of the target to the ground state of the ejectile was observed and uniquely separated from other inelastic transfer peaks in the focal plane.

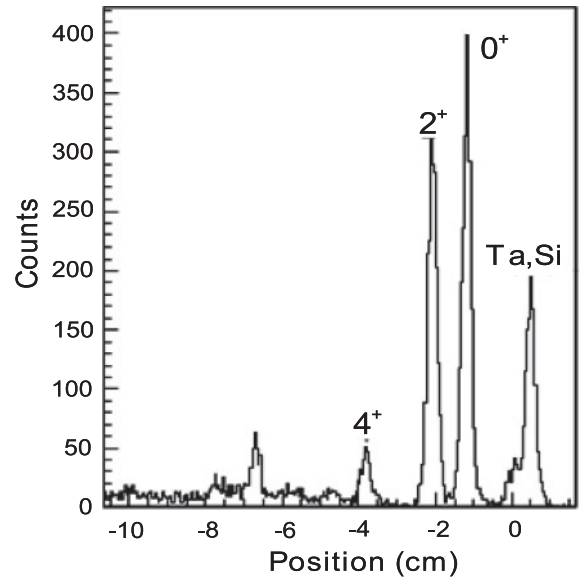

FIG. 1. Spectrum from the elastic scattering and inelastic scattering of ^{22}Ne on the ^{13}C target at $\theta_{\rm lab} = 5^\circ$. The peaks labeled 0^+, 2^+, and 4^+ are the elastic scattering and the inelastic scattering to the 2^+ and 4^+ states in ^{22}Ne, respectively, while the peak at −6.8 cm is a combination of double excitation of the target and the projectile. Ta and Si are related to heavy contaminants in the target.

The thicknesses of the ^{12}C and ^{13}C targets were measured online with two different beams, ^{22}Ne and ^{12}C, using a double-target method. First the ^{22}Ne bombarded a well-known thickness gold target. The elastic scattering (pure Rutherford) was measured with MDM at 5°. The position of the elastic peak along the dispersive x axis in the focal plane of the detector was determined. Then the ^{13}C or ^{12}C target was added in front of the Au target while keeping the spectrometer unchanged and the new position of the elastic scattering along the x axis was measured. The measured difference in positions attributable to the supplementary energy loss of the ^{22}Ne particles in the ^{13}C target was transformed into energy loss using RAYTRACE. Finally, ^{13}C thickness was determined. This value was rechecked with similar measurements using the ^{12}C beam, and also offline with a radioactive ^{228}Th α source. The average thickness of the ^{13}C target is 104 ± 8 μg/cm^2 and that of the ^{12}C target is 109 ± 9 μg/cm^2. These uncertainties include the beam integration.

III. ELASTIC AND INELASTIC SCATTERING

We have analyzed the elastic-scattering data using both phenomenological and semimicroscopic OMPs. First we used phenomenological optical potentials. They use a standard parametrization of the interaction in terms of Woods-Saxon (WS) volume form factors:

$$U(r) = -[V f_V(r) + i W f_W(r)]. \quad (1)$$

We use the heavy-ion convention for the reduced radius,

$$f_x(r) = \left[1 + \exp \frac{r - r_x\left(A_1^{1/3} + A_2^{1/3}\right)}{a_x}\right]^{-1}.$$

Only the central components have been included in the optical potential, because spin-orbit and other high-order spin-dependent couplings have been shown to have little or no influence on the shape of the angular distribution. We started with a grid search in which the depth of the real potential was varied in 10-MeV steps, while the remaining five parameters were fit. We found three to five main families of potentials, out of which we have then extracted the best solution by starting from one solution in each family and allowing the real depth to vary freely too. This kind of discrete ambiguity is typical for the strong absorption regime. The potentials within one family can be characterized by their almost common real volume integral. The jump from one family to another is almost constant.

Second, optical potentials were obtained by using a semimicroscopic double-folding model. Single-particle densities were calculated in a standard spherical Hartree-Fock procedure using the density functional of Beiner and Lombard [27] and then folded with the density- and energy-dependent effective nucleon-nucleon interaction of Jeukenne, Lejeune, and Mahaux (JLM) [28] (see Refs. [29,30] and references therein). The model produces real and imaginary potentials of independent geometries and has been shown to give good results in describing elastic-scattering data with both stable and radioactive beams, in particular in the region of p-shell nuclei. It uses only two free parameters (normalizations N_V and N_W of the real and imaginary potentials) or four (renormalizations plus two range parameters, t_V and t_W),

$$U(r) = N_V V_{DF}(r, t_V) + i N_W W_{DF}(r, t_W). \quad (2)$$

The fits in both cases were made using the code OPTIMINIX [31]. The Coulomb component in the optical potential was calculated by folding the appropriate Hartree-Fock charge densities with the proton-proton Coulomb interaction.

A. $^{12}C + ^{13}C$

Figure 2 shows the measured cross section for elastic scattering of $^{12}C + ^{13}C$ at 10.6 MeV/nucleon. The WS parameters of the OMPs obtained by fitting the data using phenomenological potentials are presented in Table I. Before comparison with the data, all calculations have been smeared with the experimentally determined angular resolution. The angular distribution given by the first parameter set in Table I, which has the smallest reduced χ^2, is plotted in Fig. 2. The optical potentials in Table I have a consistent preference for weak imaginary volume parts with almost constant absorption strength, reduced radii $r_V < r_W$, and the diffuseness parameters $a_V > a_W$. The balance among these parameters ultimately decides the survival of refractive effects in the measured distribution. The volume integrals per pair of interacting nucleons for the real and the imaginary parts of the potentials (J_V and J_W) and their root mean square (rms) radii (R_V and R_W) are included in the table. The absorption is nearly independent of the strength and shape of the real part of the potential, resulting in a constant total reaction cross section with an average value of 1457 mb. Similar results for the elastic-scattering cross sections were obtained using PTOLEMY [32].

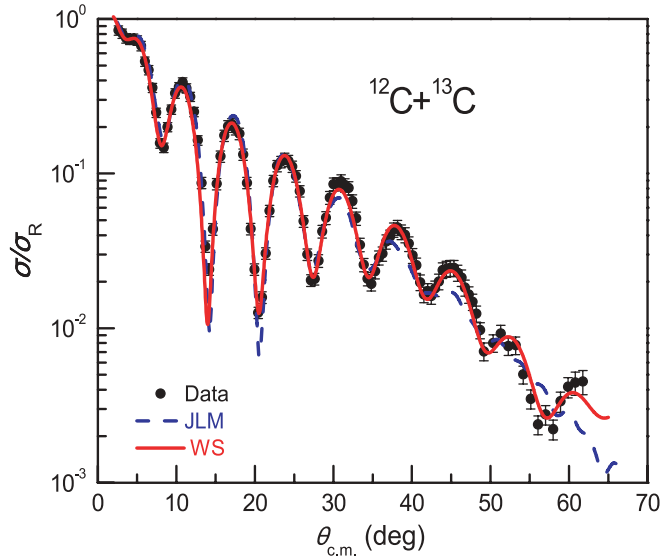

FIG. 2. (Color online) Angular distribution for elastic scattering of 127.2 MeV ^{12}C on ^{13}C. The solid and dashed curves are the calculations with the best-fit optical potentials shown in Table I for WS and double-folding form factors, respectively.

The elastic-scattering data also have been analyzed using the double-folding potential. The fitting procedure started with the standard range parameters $t_V = 1.2$ fm and $t_W = 1.75$ fm, and the average renormalization parameters $N_V = 0.37$ and

TABLE I. The best-fit parameters of the WS and semimicroscopical JLM OMPs obtained from the analysis of the elastic-scattering data for $^{12}C + ^{13}C$. R_V and R_W are the rms radii of the real and imaginary potentials, respectively. J_V and J_W are the volume integrals per interacting nucleon pair.

Potential	V (MeV)	W (MeV)	r_V (fm)	r_W (fm)	a_V (fm)	a_W (fm)	WS χ^2	σ_R (mb)	J_V (MeV fm^3)	R_V (fm)	J_W (MeV fm^3)	R_W (fm)
1	146.5	18.3	0.74	1.21	0.89	0.57	2.5	1449	269	4.26	94	4.83
2	230.7	18.9	0.65	1.19	0.89	0.60	7.8	1464	313	4.05	95	4.82
	N_V	N_W	t_V (fm)	t_W (fm)			JLM χ^2	σ_R (mb)	J_V (MeV fm^3)	R_V (fm)	J_W (MeV fm^3)	R_W (fm)
3	0.53	0.93	1.64	1.44			4.8	1458	200	4.31	115	4.40
4	0.37	1.08	1.61	1.21			4.5	1442	208	4.29	134	4.29
5	0.42	0.97	1.20	1.75			13.3	1520	236	4.08	119	4.56

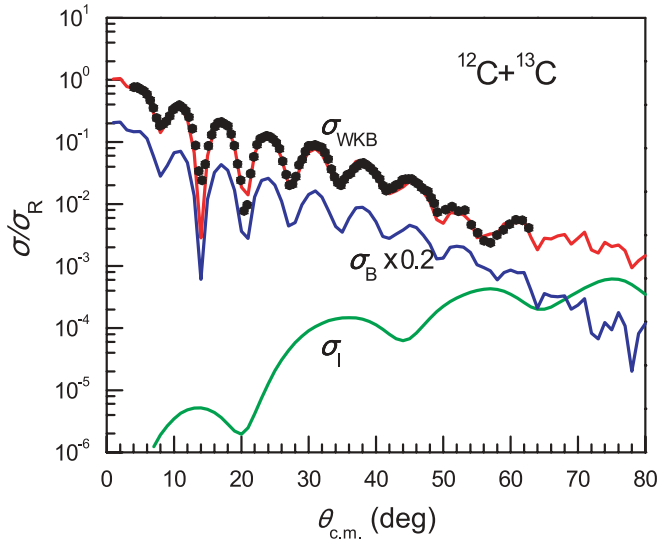

FIG. 3. (Color online) Barrier (B) internal barrier (I) decomposition of the semiclassical (WKB) cross section for the WS potential 1 in Table I. The barrier component (scaled by 0.2 in the figure) is virtually identical with the full WKB cross section, demonstrating that the reaction mechanism is entirely peripheral.

$N_W = 1.0$ of Ref. [29]. Then those parameters were adjusted until the best description of the elastic-scattering data was reached. The obtained OMP parameters are listed in Table I, and the fit of the data with the fourth parameter set is shown in Fig. 2. For the case of potential 5, the range parameters were kept fixed at $t_V = 1.20$ fm and $t_W = 1.75$ fm and only the normalizations were fitted. We find values compatible with the results of Ref. [29], obtained from the study of elastic scattering for several p-shell nuclei. The large renormalization of the real part shows that the effect of the dynamic polarization potential cannot be simply simulated by the range parameter (t_V). In contrast, the imaginary part of the optical potential does not need any renormalization, $N_W = 1.00 \pm 0.09$ [29]. This indicates that the imaginary part of the effective interaction and its density dependence are well adapted for this type of calculation. It is clear from Table I that all the double-folding potentials have similar volume integrals for the real part $J_V \approx 215$ MeV fm^3, which are equivalent to the phenomenological potentials that have real well depths with an average value around $V \approx 123$ MeV. Similar to the WS ones, the imaginary potentials are independent of the real parts, predicting a total nuclear reaction cross section around 1470 mb, which is consistent with the values found from the analysis with phenomenological potentials.

The Wentzel-Kramers-Brillouin (WKB) approximation for the scattering amplitude of Brink and Takigawa [33] is adopted here to understand the ^{12}C + ^{13}C elastic-scattering reaction mechanism. The semiclassical scattering amplitude (f_{WKB}) is decomposed into barrier (f_B) and internal barrier (f_I) amplitudes. Then the barrier and internal barrier angular distributions are calculated as $\sigma_{B,I} = |f_{B,I}|^2$. These semiclassical cross sections are compared with the data in Fig. 3. Clearly, the forward angles are dominated by the barrier component, where the Fraunhofer diffraction occurs, while the internal barrier component starts to dominate the angular distribution only at angles larger than 80°. Therefore, almost no trace of the refractive effects survives in the measured cross section, and the scattering is completely dominated by reflections at the barrier.

B. ^{22}Ne + C

A similar procedure was applied to studying the elastic scattering of ^{22}Ne + ^{13}C and ^{22}Ne + ^{12}C at a beam energy of 12 MeV/nucleon. Discrete sets of parameters are listed in Table II. The parameter sets for optical potentials 2 and 6 were obtained using an exact inversion of the phase shifts predicted by the JLM model with parameters $t_V = 1.20$, $t_W = 1.75$, $N_V = 0.34$, and $N_W = 1.22$. This procedure facilitates the use of PTOLEMY for inelastic scattering.

The calculated cross sections using the potentials that have the best fit for each of the elastic-scattering reactions are compared with the data in Fig. 4. The inelastic cross section for the ^{22}Ne*(2$^+$) + ^{12}C channel (Fig. 5) was calculated using the recommended value for the Coulomb deformation 0.562 ± 0.012 [34] and fits well the experimental data. The deformation length recipe $\beta_x R_x = \beta_c R_c$ was used to estimate the deformation for other OM components. The ^{22}Ne*(2$^+$) + ^{13}C reaction gives similar results.

For ^{22}Ne + ^{13}C, far/near-side decomposition of the scattering amplitude clarifies the oscillatory behavior of the cross section as shown in Fig. 6. At very forward angles, the near-side and Coulomb amplitudes rule the scattering and can be described by Fresnel diffraction. In the region where the far/near amplitudes are comparable, Fraunhofer diffraction develops, which gives evidence of the strong absorption. Both amplitudes are equal at $\theta = 33.5°$. Beyond this angle,

TABLE II. The parameters of the WS OMP obtained from the analysis of the elastic-scattering data for ^{22}Ne + ^{13}C and ^{22}Ne + ^{12}C.

Channel	Potential	V (MeV)	W (MeV)	r_V (fm)	r_W (fm)	a_V (fm)	a_W (fm)	χ^2	σ_R (mb)	J_V (MeV fm^3)	R_V (fm)	J_W (MeV fm^3)	R_W (fm)
^{22}Ne + ^{13}C	1	81.01	14.14	0.88	1.33	0.85	0.66	5.6	1979	155	4.74	72	5.84
	2	167.13	15.37	0.74	1.31	0.88	0.64	6.3	1937	208	4.41	74	5.73
	3	245.05	15.30	0.66	1.31	0.90	0.63	6.8	1921	234	4.26	75	5.73
^{22}Ne + ^{12}C	4	77.35	14.58	0.89	1.32	0.84	0.65	6.5	1914	154	4.70	77	5.75
	5	126.99	15.81	0.89	1.31	0.69	0.78	9.7	2095	230	4.35	83	5.92
	6	155.14	16.30	0.79	1.29	0.82	0.67	7.9	1907	223	4.34	81	5.67
	7	236.96	16.11	0.68	1.29	0.86	0.65	8.5	1874	252	4.18	80	5.64

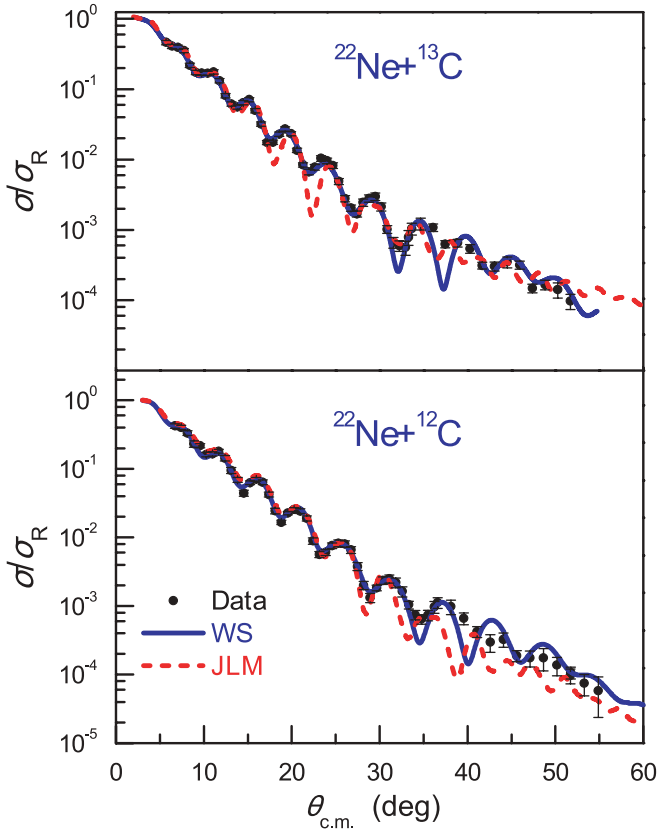

FIG. 4. (Color online) Angular distributions for the elastic scattering of ^{22}Ne + ^{13}C (top) and ^{22}Ne + ^{12}C (bottom) at 12 MeV/nucleon. The WS fit was calculated using optical potential 1 of Table II for the top panel and optical potential 4 for the bottom panel. JLM calculations were obtained using potentials 2 and 6 for the top and bottom panels, respectively.

the angular distribution is completely damped by the strong absorption. In the presence of strong absorption, only a small

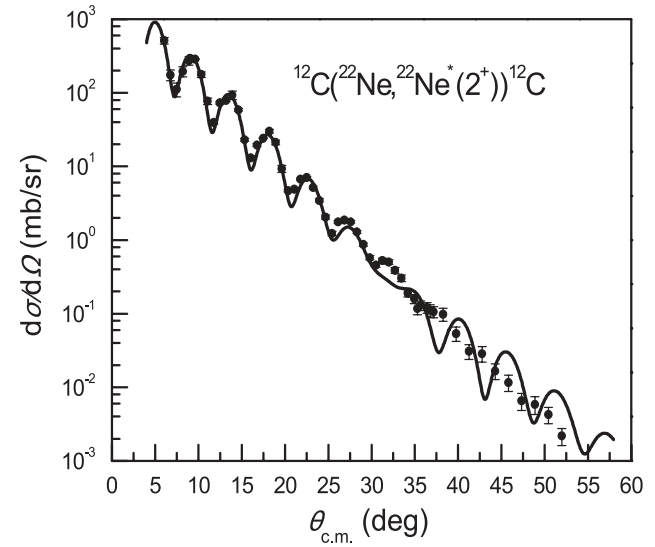

FIG. 5. Inelastic scattering angular distribution of ^{22}Ne*(2$^+$) + ^{12}C. The solid curve was calculated using optical potential 4 of Table II. Coulomb deformation is considered.

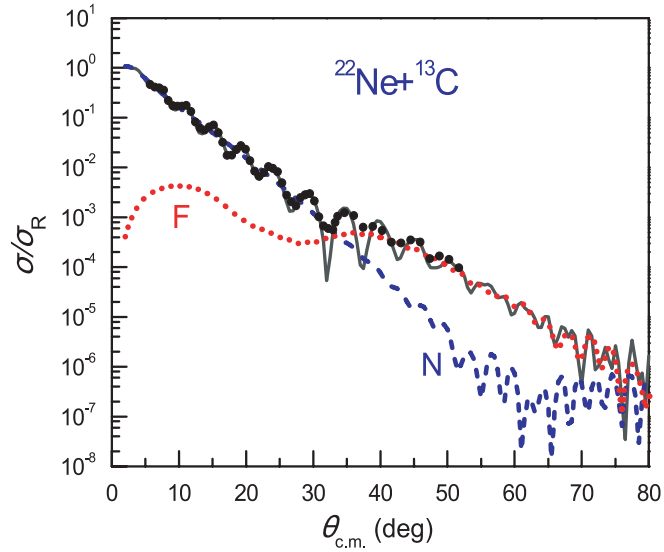

FIG. 6. (Color online) WS far-side (dots) and near-side (dashes) decomposition for ^{22}Ne + ^{13}C elastic scattering using optical potential 1 of Table II.

fraction of the scattered particle flux provides details about the interior of the nuclear potential. To clarify the reaction mechanism, a notch test was applied to estimate the radial sensitivity of the optical potential, which maps the effective region of the elastic scattering. The optical potentials in Table II were systematically perturbed with a Gaussian notch placed at selected radial distances with a strength of 10% of the bare potential and a width of 0.2 fm. Figure 7 shows that the radial sensitivity of the potential is maximized near 6.5 fm (about half-depth radius), inside the strong absorption radius of 7.9 fm. This means that the scattering is mainly sensitive to the surface region and the radius of the interaction is well determined. We have also obtained similar results for the other reactions presented in this work.

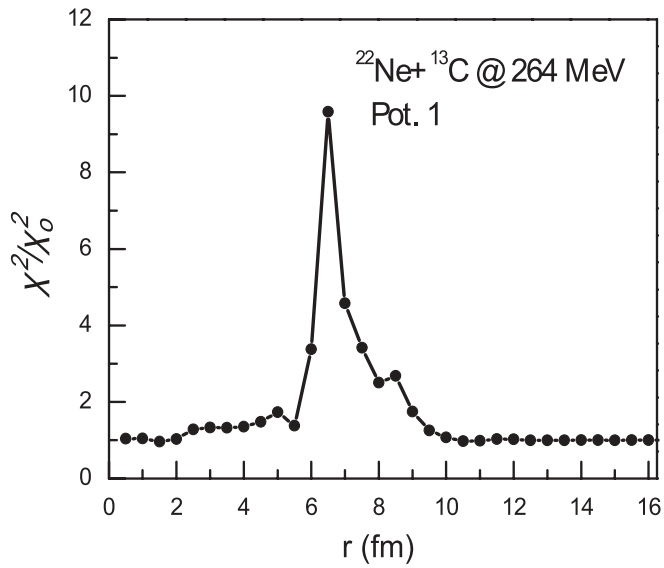

FIG. 7. Radial sensitivity test on the real potential as a function of r. The elastic scattering is sensitive to the potential in the region of strong absorption radius.

IV. ASYMPTOTIC NORMALIZATION COEFFICIENTS

We describe here the results of the analysis of the transfer reactions and how the ANCs were extracted. We start with the case of the "other vertex," $^{13}\mathrm{C} \rightarrow {}^{12}\mathrm{C} + n$, as its ANC can be extracted from this single experiment and is needed for the determination of the ANC for the vertex $^{23}\mathrm{Ne} \rightarrow {}^{22}\mathrm{Ne} + n$, which is our main goal.

A. The ^{13}C(^{12}C,^{13}C)^{12}C reaction

The angular distribution for the ^{13}C(^{12}C,^{13}C)^{12}C ground-state-to-ground-state neutron-transfer reaction is shown in Fig. 8 for a ^{12}C beam energy of E/A = 10.6 MeV/u. DWBA calculations were performed with PTOLEMY using OMP 1 from Table I for the calculation of the distorted waves in both the entrance and exit reaction channels. The calculations are shown for a binding potential of the last neutron around ^{12}C given by a WS shape with specific geometry $r_0 = 1.25$ fm and $a = 0.65$ fm and with the depth adjusted to reproduce the neutron-binding energy in ^{13}C, $\varepsilon_n = 4.946$ MeV. Normalization of the calculation to the data gives a spectroscopic factor, $S = 0.65$, from the match at forward angles $\theta_{\mathrm{c.m.}} \leqslant 18^\circ$. It is known that the extracted value of the spectroscopic factor is strongly dependent on the choice of the binding potential parameters (r_0, a). Recent reanalysis of the angular distribution of $p_{1/2}$ to $p_{1/2}$ transitions of ^{12}C(d,p)^{13}C and ^{13}C(p,d)^{12}C neutron-transfer reactions performed at several incident deuteron energies (12 to 60 MeV) gave an average value $S = 0.61 \pm 0.09$ [35]. This agrees with our measured value, but only when the same geometries of the WS are used. On the other hand, excitation of the 4.44 MeV 2^+ state in ^{12}C or of the 3.09 MeV $1/2^+$ state in ^{13}C may contribute to the population of the ground state of ^{13}C in the transfer reaction. A study of ^{12}C(d,p)^{13}C and ^{13}C(p,d)^{12}C reactions

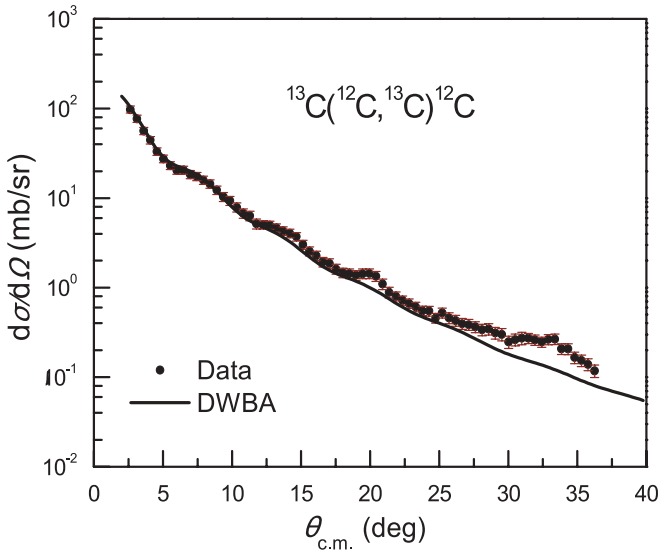

FIG. 8. Experimental and the calculated angular distribution of the ^{13}C(^{12}C,^{13}C)^{12}C transfer reaction. The points are the experimental data, while the solid line is the DWBA cross section obtained from PTOLEMY.

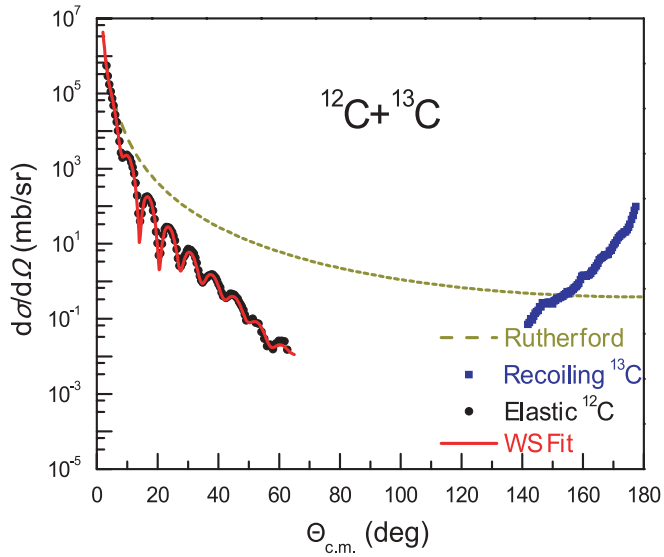

FIG. 9. (Color online) The whole angular range $\Theta_{\mathrm{c.m.}} = 0^\circ$–$180^\circ$ of the $^{12}\mathrm{C} + {}^{13}\mathrm{C}$ elastic-scattering cross section. The data (black dots) at forward angles indicate the elastically scattered ^{12}C particles. Those at backward angles (blue squares) were obtained by measuring the recoiling ^{13}C nuclei at complementary forward angles. The dashed line is the Rutherford scattering cross section. The WS fit (red line) has been obtained using potential 1 of Table I.

beyond the Born approximation for energies between 7 and 60 MeV (Ref. [36]) found that coupling to these states may increase the amplitude of the cross section up to 15% at low deuteron energies, $E_d \leqslant 30$ MeV, and is negligible at higher energies. The coupled reaction channel effects have been neglected in the present calculations of the ^{13}C(^{12}C,^{13}C)^{12}C exchange reaction.

Measuring ^{13}C ground-state nuclei from the neutron exchange reaction at forward angles is kinematically equivalent to measuring elastically scattered ^{12}C particles at backward angles in the c.m. frame. Therefore, their amplitudes may interfere. The angular distribution for the elastic scattering of ^{12}C on ^{13}C using the data from the detection of ^{12}C in the forward hemisphere and the data from the detection of ^{13}C at complementary forward angles in the backward hemisphere are plotted in Fig. 9. The rise in the cross section at backward angles demonstrates that the reaction mechanism is different from potential scattering and therefore can be explained solely by the transfer of a neutron from the target to the projectile. Hence, the two mechanisms dominate in different angular regions, and we can neglect interference between the elastic and the exchange amplitudes. Because the entrance and exit channels of the ^{13}C(^{12}C,^{13}C)^{12}C reaction are identical, the ANC can be obtained using

$$\frac{d\sigma}{d\Omega} = C^4_{p_{1/2}}(^{13}\mathrm{C})\frac{\sigma^{\mathrm{DWBA}}}{b^4_{p_{1/2}}}, \tag{3}$$

where in the calculation the neutron is transferred from the $p_{1/2}$ orbital in the target to the same orbital in the ^{13}C ejectile, and its ANC is $C^2_{p_{1/2}}$. The value of the single-particle ANC $b_{p_{1/2}}$ was obtained from the ratio between the normalized single-particle bound-state neutron $p_{1/2}$ wave function and the

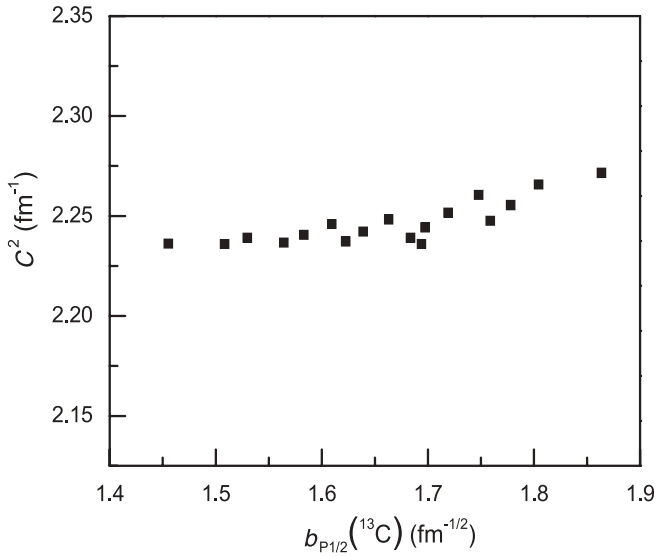

FIG. 10. ANC C^2 for the ^{13}C(^{12}C,^{13}C)^{12}C reaction as a function of the bound-state single-particle ANC b.

corresponding Hankel function at radii greater than 4.5 fm. The spectroscopic factor is given by $S_{p_{1/2}} = C^2_{p_{1/2}}/b^2_{p_{1/2}}$. The procedure was repeated with different geometries (r_0, a) of the neutron-binding potential. The relation between the extracted $C^2_{p_{1/2}}$ and the single-particle ANC $b_{p_{1/2}}$ for single-particle potentials with parameters ranging from $r_0 = 1.1$–1.3 fm and $a = 0.50$–0.65 fm is plotted in Fig. 10. In each case, the depth of the single-particle potential was adjusted to fit the experimental neutron-binding energy. The ANC varies by less than $\pm 2\%$ over the full range considered. In contrast, S, which is inversely proportional to b^2, varies by more than 30%. This can be understood by recognizing that the transfer is peripheral, and therefore the calculated cross section σ^{DWBA} is to a good approximation proportional to $(b^2)^2$. Reversing the reasoning, this constancy of C^2 means that only the asymptotic part of the wave function contributes in the DWBA calculation and the transfer reaction is peripheral. A spin-orbit interaction was considered, here and throughout the article, in the proton-binding potential used to calculate the single-particle wave functions used. We have used a standard surface type $1/r \times (df/dr) \times$ LS, with the same WS geometry $f(r_0,a)$ as the volume part and with the strength $=$ 18.6 MeV fm^2 obtained by us earlier in a careful study of bare single-particle levels in the region of ^{56}Ni [37]. However, this spin orbit does not affect at all the ANC results, because the reaction is peripheral and only the asymptotic part in the wave function matters.

By normalizing the calculated DWBA cross section to the measured one, the value of the ANC for the virtual decay $^{13}\mathrm{C(g.s.)} \rightarrow {}^{12}\mathrm{C} + n$ is extracted using Eq. (3). The most important angular region for which to obtain the ANC is small angles, where the cross section is dominated by one-step effects and the calculated shape of the angular distribution does not depend on the geometry of the bound-state WS potentials. We consider the region $\theta_{\mathrm{c.m.}} < 18^\circ$. The uncertainties in the value of C^4 include the contribution of the average statistical errors (3%), the normalization of cross section with the Faraday cup (3%), the measurements of the target thickness (7.5%), the geometry of the neutron-binding potential used in the DWBA calculations (1.5%), the fit between the measured and the calculated cross sections for several angular ranges (1.0%), and the normalization of the cross section with different optical potentials in Table I (1.5%). All these uncertainties are summed in quadrature to give an overall 9% accuracy of C^4, so the uncertainty in determining C^2 is 4.5%. As a result from the present experiment, the extracted ANC is $C^2_{p_{1/2}} = 2.24 \pm 0.11$ fm^{-1}. A value for the ANC from the analysis of ^{12}C + ^{13}C elastic scattering, ^{13}C(p,d)^{12}C(g.s.), ^{12}C(d,p)^{13}C(g.s.), ^{13}C(d,t)^{12}C, ^{13}C(^{12}C,^{13}C)^{12}C, and ^{12}C(^{13}C,^{12}C)^{13}C reactions (where g.s. stands for ground state) has an average value of $C^2_{p_{1/2}} = 2.40 \pm 0.12$ fm^{-1} [20,21]. This value is in good agreement with the value obtained in this experiment, but a more precise value for the ANC is obtained by calculating the weighted average of all the measurements. Therefore, we adopt $C^2_{p_{1/2}} = 2.31 \pm 0.08$ fm^{-1} and use this value later in this article.

B. The ^{13}C(^{22}Ne,^{23}Ne)^{12}C reaction

The angular distributions for the ^{13}C(^{22}Ne,^{23}Ne)^{12}C reaction for neutron transitions from the $1/2^-$ ground state of ^{13}C to the $5/2^+$ (ground state) and $1/2^+$ ($E^* = 1.017$ MeV) states in ^{23}Ne are shown in Fig. 11. The DWBA transfer reaction cross sections were calculated with PTOLEMY by using the OMPs from Table II, where parameters for $^{22}\mathrm{Ne} + {}^{13}\mathrm{C}$ were used in the entrance channel of the reaction, while those for $^{22}\mathrm{Ne} + {}^{12}\mathrm{C}$ were employed for the distorted waves in the exit channel. Using the geometrical parameters $r_0 = 1.25$ fm and $a = 0.65$ fm of the neutron-binding potential, fits of the DWBA calculations to the data are also shown in Fig. 11. A systematic angular phase shift of about 0.2° in the laboratory system was observed between the data and the DWBA transfer reaction cross sections. Measurements for the transfer reaction were taken concurrently with $^{22}\mathrm{Ne} + {}^{13}\mathrm{C}$ elastic and inelastic scatterings, neither of which allow such a shift. Thus, we conclude that the phase shifts for the neutron-transfer reactions are not instrumental in nature. The cross section of $^{22}\mathrm{Ne} + {}^{13}\mathrm{C}(J^\pi = 1/2^+,\ 3.09\ \mathrm{MeV}) \rightarrow {}^{23}\mathrm{Ne} + {}^{12}\mathrm{C}$ leads to an angular distribution that has oscillations that are out of phase with the direct ground-state-to-ground-state transfer reaction, while the calculated $^{22}\mathrm{Ne}(J^\pi = 2^+, 1.275\ \mathrm{MeV}) + {}^{13}\mathrm{C} \rightarrow {}^{23}\mathrm{Ne} + {}^{12}\mathrm{C}$ reaction has an in-phase angular distribution. Coupled-channel Born approximation calculations did not provide any improvement. A similar angle shift was seen, but not resolved, for proton transfer from the p shell to the sd shell in the ^{13}C(^{7}Li,^{6}He)^{14}N [38] and ^{13}C(^{14}N,^{13}C)^{14}N [39] reactions. Therefore, the 0.2° shift will be treated as a systematic uncertainty in the final value of the ANC. The ANC for the $d_{5/2}$ component in the ^{13}C(^{22}Ne,^{23}Ne(g.s.))^{12}C reaction was extracted using the following equation:

$$\frac{d\sigma}{d\Omega} = C^2_{p_{1/2}}(^{13}\mathrm{C})C^2_{d_{5/2}}(^{23}\mathrm{Ne})\frac{\sigma^{\mathrm{DWBA}}}{b^2_{p_{1/2}}(^{13}\mathrm{C})b^2_{d_{5/2}}(^{23}\mathrm{Ne})}. \quad (4)$$

An analysis similar to that illustrated in Fig. 10 finds that $C^2_{d_{5/2}}$ varies less than 3% when the geometry of the single-particle potential is modified. Hence, the reaction is peripheral. The

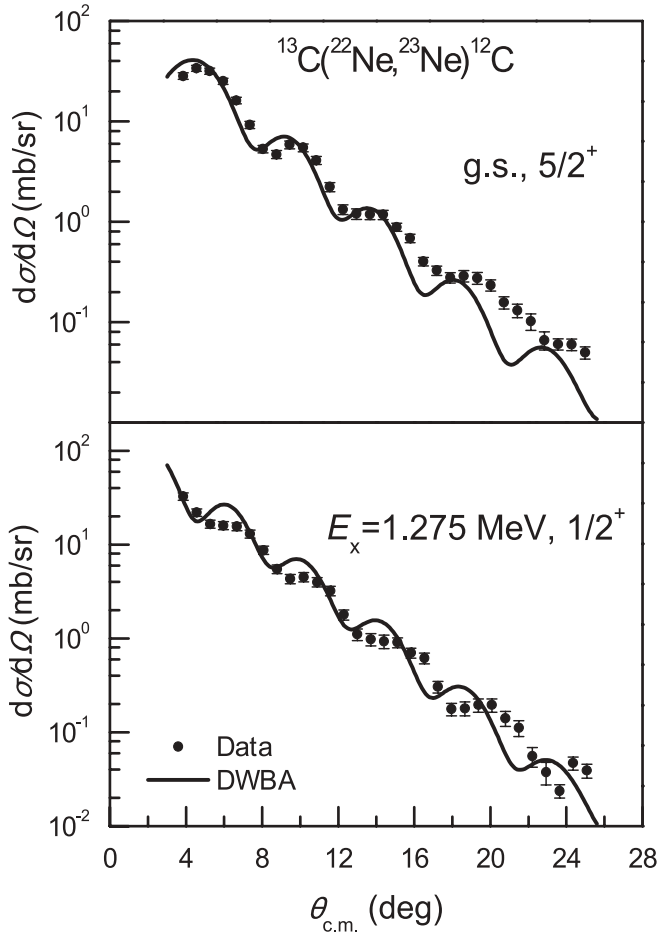

FIG. 11. Angular distributions for the ^{13}C(^{22}Ne,^{23}Ne)^{12}C reaction. (Top) A neutron transfer to the ground state of ^{23}Ne. (Bottom) A transfer to the first excited state of ^{23}Ne. The DWBA curves were calculated using optical potentials 1 and 4 from Table II for the incident and outgoing channels, respectively.

ANCs were extracted by fitting the calculation to the data up to $\theta_{\rm c.m.} = 16^\circ$. The uncertainty in the value of the $C^2_{d_{5/2}}$ includes 3% from the determination of the ANC $C^2_{p_{1/2}}(^{13}\mathrm{C})$ of the other vertex of the reaction, the normalization of cross section with the Faraday cup (3%), 7.5% from the measurement of the target thickness, 2% from the geometry of the neutron-binding potential used in the DWBA calculation, 1.5% from calculating the cross section with several permutations of entrance versus exit optical potentials in Table II, and 3% statistical errors. Therefore, the overall uncertainty in determining the $C^2_{d_{5/2}}$ is about 9%. Similar conclusions were drawn for the $1/2^+$ first excited state. The systematic uncertainty attributable to the 0.2° angle shift in the angular distributions was also calculated. The angles of the transfer reaction cross section were reduced by 0.56° in the c.m. system. A new normalization between the DWBA and the data cross sections showed that the fit was dramatically improved up to $\theta_{\rm c.m.} = 19^\circ$ but the value of $C^2_{d_{5/2}}$ was decreased by 14%. Similar calculations showed that the $C^2_{s_{1/2}}$ was changed by almost 20%. In conclusion, the ANCs in ^{23}Ne are $C^2_{d_{5/2}} = 0.86 \pm 0.08 \pm 0.12$ fm^{-1} for the ground state and $C^2_{s_{1/2}} = 18.2 \pm 1.8 \pm 3.8$ fm^{-1} for the first excited state. These values or their corresponding nuclear vertex constants have not been previously measured experimentally. Earlier model calculations give ranges of 0.71–0.81 fm^{-1} for $C^2_{d_{5/2}}$ and 16.30–18.49 fm^{-1} for $C^2_{s_{1/2}}$, as reported in Refs. [40] and [41], respectively. Our experimental results are consistent with these calculations.

V. ASTROPHYSICAL REACTION RATES

The ANC for the ground state in ^{23}Al was obtained from the corresponding ANC determined in ^{23}Ne using the assumption that they have identical spectroscopic factors (mirror symmetry):

$$S_{d_{5/2}}(^{23}\mathrm{Al}) = S_{d_{5/2}}(^{23}\mathrm{Ne}) \Rightarrow$$
$$C^2_{d_{5/2}}(^{23}\mathrm{Al}) = \frac{b^2_{d_{5/2}}(^{23}\mathrm{Al})}{b^2_{d_{5/2}}(^{23}\mathrm{Ne})} C^2_{d_{5/2}}(^{23}\mathrm{Ne}). \quad (5)$$

Using a WS potential with $r_0 = 1.25$ fm and $a = 0.65$ fm, the obtained spectroscopic factor is 0.43, which is bit larger than the 0.34 value calculated using OXBASH [42]. The single-particle ANC, b, in ^{23}Al was calculated for a proton bound with the same geometry and the same spin-orbit interaction as were used for a neutron bound in ^{23}Ne. Only the depth of the central potential was adjusted to reproduce the experimental proton-binding energy in ^{23}Al, $\varepsilon_p = 143(6)$ keV deduced from the ^{23}Al mass evaluated in Ref. [17]. The value obtained for the depth of the nuclear potential by imposing this procedure is similar to the depth of the nuclear potential found for ^{23}Ne. This is a confirmation of the charge symmetry assumption made here. The value of $b_{\ell j}$ strongly depends on the geometrical parameters r_0 and a assumed for the potentials. However, the ratio $b_{\ell j}(^{23}\mathrm{Al})/b_{\ell j}(^{23}\mathrm{Ne})$ is independent of these parameters of the potential that binds the proton or the neutron around its corresponding core. We find that this ratio is equal to 73.4 for $1d_{5/2}$ (the major component of the $J^\pi = 5/2^+$ ground state). A 3% uncertainty is assigned to this ratio to account for possible charge-symmetry breaking effects [15]. Inserting this ratio and the value of the ANC in ^{23}Ne, which was obtained in the previous section, into Eq. (5), we find $C^2_{d_{5/2}}(^{23}\mathrm{Al}) = (4.63 \pm 0.77) \times 10^3$ fm^{-1}. We should note that while this seems unusually large, that is because of the small value of the corresponding Whittaker function, related to the very small proton binding energy in ^{23}Al. This is the first measurement to determine the ANC in ^{23}Al.

The ^{22}Mg$(p,\gamma)^{23}$Al direct-capture reaction rate has been estimated using RADCAP [43]. The depth V_o of the proton nuclear binding potential with the same geometry as used previously in the DWBA calculations for the transfer reaction was adjusted so that the binding energy of the ground state is reproduced. The bound-state wave function was then calculated and used to determine the astrophysical S factor at each energy E for a direct, one-step transition from a continuum state to the $1d_{5/2}$ single-particle bound state. The proton-capture cross section ($\sigma_{\rm dir}$), which was calculated assuming only the electromagnetic

transition $E1$, can be expressed by

$$\sigma_{\rm dir} = C^2 \frac{\tilde{\sigma}_{\rm RADCAP}}{b^2}, \tag{6}$$

where $\tilde{\sigma}$ is the cross section calculated by RADCAP. We find that $\tilde{\sigma}_{\rm RADCAP}/b^2$ is nearly independent of the geometry of the single-particle WS potential. Therefore, the ANC $C^2_{d_{5/2}}$ is the important parameter for determining the S factor. We find that at $E = 0$ MeV, $S(0) = 0.96 \pm 0.11$ keV b. It was reported in Ref. [44] that $S(0) = 0.66$ keV b, which is about 30% less than our value. This is attributable to different values of the spectroscopic factors, but mostly to the new value found for the binding energy ε_p used in the calculations. The calculated S factor as a function of energy for ^{22}Mg$(p,\gamma)^{23}$Al can be parameterized with a simple polynomial dependence, $S(E) = 0.96 + 0.15E + 0.78E^2 - 0.60E^3$ (E in MeV). When the uncertainties of $S(0)$ for ^{22}Mg(p,γ) reaction are included, then the upper and lower limits of $S(E)$ are, respectively, $S_{\rm upper}(E) = 1.07 + 0.19E + 0.78E^2 - 0.58E^3$ and $S_{\rm lower}(E) = 0.86 + 0.15E + 0.63E^2 - 0.47E^3$. Taking the central energy of the Gamow peak for $p + ^{22}$Mg at $E_o = 0.63T_9^{2/3}$ MeV, then the effective S factor [45] in terms of T_9 is given by

$$S_{\rm eff}(T_9) = 0.96\big[1 + 0.019T_9^{1/3} + 0.098T_9^{2/3} + 0.013T_9 + 0.321T_9^{4/3} + 0.108T_9^{5/3}\big]. \tag{7}$$

With this equation, the direct-capture rate for ^{22}Mg$(p,\gamma)^{23}$Al is

$$N_A\langle\sigma\upsilon\rangle = 37.78\left(\frac{21.92}{T_9^{1/3}}\right)^2 S_{\rm eff}(T_9)e^{-21.92/T_9^{1/3}}. \tag{8}$$

In addition to the direct-capture reaction, the resonant contribution through the first excited state $J^\pi = 1/2^+$ of ^{23}Al has been calculated. Its measured excitation energy is 0.528(19) MeV [44], and with the new ^{23}Al mass from Ref. [17], the resonance energy becomes $E_r = 0.385(20)$ MeV. The proton width of this resonance is much greater than the γ width, so the strength of the resonance is proportional to Γ_γ. Its experimental value, $\Gamma_\gamma = 7.2 \pm 1.4 \times 10^{-7}$ eV, which was obtained from the Coulomb dissociation of ^{23}Al at 50 MeV/u [46], is adopted here to evaluate the resonant reaction rate, which is given by

$$N_A\langle\sigma\upsilon\rangle = 0.12T_9^{-3/2}\exp\left(-\frac{4.47}{T_9}\right). \tag{9}$$

Both the direct and the resonant capture reaction rates are plotted in Fig. 12. In the range $T_9 = 0.2$–0.4, which is typical for ONe novae, the direct and resonant terms are comparable, while for $T_9 > 0.6$ or $T_9 < 0.2$, the direct capture dominates the reaction rate.

We have compared the total reaction rate, which adds the direct and resonant terms, with previous estimates by Wiescher *et al.* [13], Caggiano [44], and He *et al.* [47]. All three calculate the same direct-capture contributions. At the temperatures relevant for ONe novae the resonant yields differ, with Wiescher *et al.*'s being the largest and Caggiano's the smallest. The new reaction rate is similar to Wiescher *et al.*'s estimate and is almost two times larger than Caggiano's determinations. This

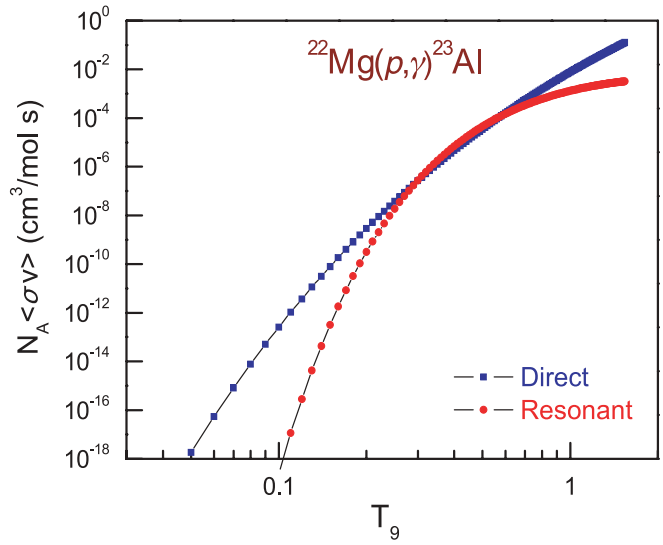

FIG. 12. (Color online) Direct and resonant capture rate contributions to the ^{22}Mg$(p,\gamma)^{23}$Al reaction. The two rates are competitive for temperatures $T_9 = 0.2$–0.45 in ONe novae. Otherwise, the direct capture dominates the reaction rate.

difference is mainly attributable to the binding energy of the proton in ^{23}Al and the spectroscopic factors, or their equivalent ANCs, that are used in the present reaction rate calculations. Because these rates are comparable, the astrophysical implications of the new reaction rate for the nucleosynthesis of ^{22}Na are similar and can be inferred from this and previous works. It was shown by Caggiano that the production of ^{22}Na compensates the loss of ^{22}Mg. This leads to a small mass fraction increase of ^{23}Al, but it explains less than half of the ^{22}Mg loss. However, the low Q value of the ^{22}Mg$(p,\gamma)^{23}$Al reaction may make the proton-capture process balance easily with its photodisintegration reaction ^{23}Al$(\gamma,p)^{22}$Mg. Alternatively, the ^{23}Al$(p,\gamma)^{24}$Si reaction has been studied to determine the $2p$-capture rate on ^{22}Mg [48] to understand the low production of ^{23}Al. The latter shows that the depletion of ^{22}Mg is larger by a factor of two than its β decay to ^{22}Na only when $T_9 \sim 0.45$ and the density is in excess of 10^4 g/cm^3. These conditions may occur in massive novae such as $1.35M_\odot$ ONe white-dwarf novae. For $1.25M_\odot$, where $T_9 \sim 0.35$ and $\rho \approx 10^2$–10^4 g/cm^3, the $2p$-capture process produces only limited amounts of ^{23}Al and ^{24}Si that could not explain the missing signature of ^{22}Na. Therefore, the probability of the proton capture in ^{22}Mg may be larger than its β decay only when extreme density and temperature conditions take place in novae. This argues that the ^{22}Mg$(p,\gamma)^{23}$Al reaction may be more important in X-ray bursts, as suggested in Ref. [49]. Nevertheless, our rate for this reaction has impact on the nucleosynthesis of ^{22}Na and should be included in the database of the reaction rates for novae.

VI. CONCLUSIONS

We have measured two different neutron-transfer reactions: ^{13}C$(^{12}$C,^{13}C$)^{12}$C and ^{13}C$(^{22}$Ne,^{23}Ne$)^{12}$C. The elastic scattering for both reactions were also measured over a wide angular range. A detailed classical OM analysis in terms of

both phenomenological and semimicroscopic folding form factors, which include modern energy- and density-dependent nucleon-nucleon effective interactions, allowed a precise determination of optical potentials to be used in DWBA analysis of the transfer reactions, and thus a more precise determination of the relevant ANCs. The reaction mechanism revealed by an exact semiclassical decomposition of the scattering amplitudes demonstrates that the reactions are highly peripheral and leads to reliable ANCs. The measurements of the ^{13}C(^{12}C,^{13}C)^{12}C reaction were used to obtain the ANC of the ground state of ^{13}C into the channel $^{12}C + n$, which is needed to extract the ANCs for the ground state and first excited state in ^{23}Ne using the second reaction. The neutron ANC found here for ^{23}Ne has been transposed into the proton ANC for the corresponding state in the mirror nucleus ^{23}Al. Then it has been used to determine the astrophysical reaction rate for ^{22}Mg(p,γ)^{23}Al and to investigate its effects on the nucleosynthesis of ^{22}Na in ONe novae. We found that the presently determined reaction rate does not differ considerably from the ones used before, based on scarcer experimental data. Therefore, we reach the same conclusion that this reaction cannot explain the nonobservation by satellite telescopes of the γ-ray line from the decay in ^{22}Na following novae explosions. Radiative proton capture on ^{22}Mg is only important for the depletion of ^{22}Na in massive novae, at larger temperatures and densities.

ACKNOWLEDGMENTS

This work was supported in part by the US Department of Energy under Grant Nos. DE-FG02-93ER40773 and DE-FG52-06NA26207, the NSF under Grant No. PHY-0852653, the Robert A. Welch Foundation under Grant No. A-1082, and by CNCSIS (Romania) Grant No. PN-II-PCE-2007-1/258.

[1] P. Gil-Pons and E. García-Berro, Astron. Astrophys. **375**, 87 (2001).
[2] C. Iliadis, A. Champagne, J. José, S. Starrfield, and P. Tupper, Astrophys. J. Suppl. **142**, 105 (2002).
[3] R. D. Gehrz, J. W. Truran, R. E. Williams, and S. Starrfield, Publ. Astron. Soc. Pac. **110**, 3 (1998).
[4] M. Livio and J. W. Truran, Astrophys. J. **425**, 797 (1994).
[5] D. C. Black, Geochim. Cosmochim. Acta **36**, 347 (1972).
[6] M. Arnould and W. Beelen, Astron. Astrophys. **33**, 215 (1974); M. Arnould and H. Norgaard, *ibid.* **64**, 195 (1978).
[7] A. F. Iyudin *et al.*, Astron. Astrophys. **300**, 422 (1995).
[8] V. Schönfelder *et al.*, Astron. Astrophys. Suppl. Ser. **143**, 145 (2000).
[9] A. J. Bird *et al.*, Astrophys. J. **636**, 765 (2006).
[10] S. Bishop *et al.*, Phys. Rev. Lett. **90**, 162501 (2003).
[11] J. M. D'Auria *et al.*, Phys. Rev. C **69**, 065803 (2004).
[12] S. Seuthe *et al.*, Nucl. Phys. A **514**, 471 (1990).
[13] M. Wiescher, J. Görres, B. Sherrill, M. Mohar, J. S. Winfield, and B. A. Brown, Nucl. Phys. A **484**, 90 (1988).
[14] H. M. Xu, C. A. Gagliardi, R. E. Tribble, A. M. Mukhamedzhanov, and N. K. Timofeyuk, Phys. Rev. Lett. **73**, 2027 (1994).
[15] L. Trache, A. Azhari, F. Carstoiu, H. L. Clark, C. A. Gagliardi, Y.-W. Lui, A. Mukhamedzhanov, X. Tang, N. Timofeyuk, and R. E. Tribble, Phys. Rev. C **67**, 062801(R) (2003).
[16] N. K. Timofeyuk, R. C. Johnson, and A. M. Mukhamedzhanov, Phys. Rev. Lett. **91**, 232501 (2003).
[17] V. E. Iacob, Y. Zhai, T. Al-Abdullah, C. Fu, J. C. Hardy, N. Nica, H. I. Park, G. Tabacaru, L. Trache, and R. E. Tribble, Phys. Rev. C **74**, 045810 (2006).
[18] M. B. Tsang, J. Lee, and W. G. Lynch, Phys. Rev. Lett. **95**, 222501 (2005).
[19] P. Mohr, H. Herndl, and H. Oberhummer, Phys. Rev. C **55**, 1591 (1997).
[20] H. P. Gubler, G. R. Platner, I. Sick, A. Traber, and W. Weiss, Nucl. Phys. A **284**, 114 (1977).
[21] A. M. Mukhamedzhanov and N. Timofeyuk, Sov. J. Nucl. Phys. **51**, 431 (1990) [Yad. Fiz. **51**, 679 (1990)].
[22] D. H. Youngblood and J. D. Bronson, Nucl. Instrum. Methods Phys. Res. A **361**, 37 (1995).
[23] D. M. Pringle, W. N. Catford, J. S. Winfield, D. G. Lewis, N. A. Jelley, K. W. Allen, and J. H. Coupland, Nucl. Instrum. Methods Phys. Res. A **245**, 230 (1986).
[24] A. M. Mukhamedzhanov *et al.*, Phys. Rev. C **56**, 1302 (1997).
[25] J. S. Winfield, D. M. Pringle, W. N. Catford, D. G. Lewis, N. A. Jelley, and K. W. Allen, Nucl. Instrum. Methods Phys. Res. A **251**, 297 (1986).
[26] S. Kowalski and H. A. Enge, computer code RAYTRACE, 1986 (unpublished).
[27] M. Beiner and R. J. Lombard, Ann. Phys. (NY) **86**, 262 (1974).
[28] J. P. Jeukenne, A. Lejeune, and C. Mahaux, Phys. Rev. C **16**, 80 (1977).
[29] L. Trache, A. Azhari, F. Carstoiu, H. L. Clark, C. A. Gagliardi, Y.-W. Lui, A. M. Mukhamedzhanov, and R. E. Tribble, Phys. Rev. C **61**, 024612 (2000).
[30] F. Carstoiu, L. Trache, R. E. Tribble, and C. A. Gagliardi, Phys. Rev. C **70**, 054610 (2004).
[31] F. Carstoiu, computer code OPTIMINIX, 1996 (unpublished).
[32] M. Rhoades-Brown, M. McFarlane, and S. C. Pieper, Phys. Rev. C **21**, 2417 (1980); **21**, 2436 (1981).
[33] D. M. Brink and N. Takigawa, Nucl. Phys. A **279**, 159 (1977).
[34] S. Raman, C. W. Nestor J. R., and P. Tikkanen, At. Data Nucl. Data Tables **78**, 1 (2001).
[35] X. D. Liu, M. A. Famiano, W. G. Lynch, M. B. Tsang, and J. A. Tostevin, Phys. Rev. C **69**, 064313 (2004).
[36] F. Delaunay, F. M. Nunes, W. G. Lynch, and M. B. Tsang, Phys. Rev. C **72**, 014610 (2005).
[37] L. Trache *et al.*, Phys. Rev. C **54**, 2361 (1996).
[38] J. Cook, M. N. Stephens, and K. W. Kemper, Nucl. Phys. A **466**, 168 (1987).
[39] L. Trache, A. Azhari, F. Carstoiu, H. L. Clark, C. A. Gagliardi, Y.-W. Lui, A. M. Mukhamedzhanov, and R. E. Tribble, Phys. Rev. C **58**, 2715 (1998).
[40] N. K. Timofeyuk and P. Descouvemont, Phys. Rev. C **71**, 064305 (2005).
[41] N. K. Timofeyuk and P. Descouvemont, Phys. Rev. C **72**, 064324 (2005).
[42] B. A. Brown, A. Etchegoyen, W. D. M. Rae, and N. S. Goodwin, Michigan State University Cyclotron Laboratory Internal Report No. MSUCL-524, 1986.

[43] C. A. Bertulani, Comput. Phys. Commun. **156**, 123 (2003).
[44] J. A. Caggiano *et al.*, Phys. Rev. C **64**, 025802 (2001).
[45] C. E. Rolfs and W. S. Rodney, *Cauldrons in the Cosmos* (University of Chicago Press, Chicago, 1986).
[46] T. Gomi *et al.*, Nucl. Phys. A **718**, 508c (2003).
[47] J. J. He *et al.*, Phys. Rev. C **76**, 055802 (2007).
[48] H. Schatz *et al.*, Phys. Rev. Lett. **79**, 3845 (1997).
[49] J. José and M. Hernanz, Eur. Phys. J. A **27**, 107 (2006).